JOURNAL OF AEROSPACE SOCIETY MALAYSIA

ARTICLE

EXPERIMENTAL WIND TUNNEL TESTING OF SHARP-EDGED DELTA WING UNDER ROLLING AND PITCHING MOTION

Naderaj Vellan [1,*], Sakib Islam Fahim [1], Syazana Emran [1] and Shabudin Mat [2]

1. Faculty of Mechanical Engineering, Universiti Teknologi Malaysia, Malaysia.
2. UTM Aerolab, Institute for Sustainable Transport, Universiti Teknologi Malaysia, Malaysia.

*Correspondence: v.nadarraj@gmail.com

Abstract: This study presents an experimental investigation of aerodynamic characteristics of a sharp-edged delta wing that is undergoing controlled rolling and pitching motions in a low-speed wind tunnel. Delta wings have been distinguished by their distinctive capacity to maintain lift at high angles of attack as a result of formation of leading-edge vortices. The wind tunnel tests were conducted in the Universiti Teknologi Malaysia's Low-Speed Tunnel with a freestream velocity of 25 m/s, which corresponds to a Reynolds number of 1.288×10^6 based on the wing model's root chord. In the experiments, the delta wing model, designed with a 65° sweep angle, was subjected to sinusoidal rolling and pitching motions at amplitudes of 10° and frequencies of 1000 Hz. The surface pressure distributions were obtained by using an array of 106 pressure taps and they were corrected for solid blockage using the Maskell method. On the whole, the results reveal that unsteady motions significantly influence the vortex development, symmetry and breakdown location, with phase lags observed between the motion and the aerodynamic response. These findings provide an essential benchmark data for computational fluid dynamics (CFD) validation and aerodynamic design of maneuvering delta-wing configurations.

Keywords: delta wing, pitching motion, rolling motion, unsteady aerodynamics, vortex dynamics, wind tunnel testing

1. Introduction

Delta wings are a critical aerodynamic configuration in modern aerospace design as they are prized for their capability to maintain lift at high angles of attack through the formation of strong leading-edge vortices (LEVs). By postponing stall and enhancing maneuverability, the vortices further contribute to an enhanced aerodynamic performance of the aircraft. This vortex-dominated flow regime enables the superior maneuverability and high-lift performance, making delta wings the preferred choice for high-speed aircraft, unmanned aerial vehicles and agile platforms [1].

In steady conditions, the aerodynamics of delta wings can be taken to be already well understood, with classical works such as Gursul et al. that provides the foundation for vortex behavior in the non-slender configurations [2]. Moreover, several recent studies have expanded this understanding using high-fidelity experimental and numerical techniques. For instance, Zamzuddin et al. showed that sharp-edged delta wings exhibit notable changes in vortex stability when subjected to flow control via blowing [3]. However, it has been noted that the LEVs are highly sensitive to unsteady motions such as rolling and pitching, which can significantly alter the lift, drag and stability characteristics of the aircraft. These vortices are subject to intricate interactions that can result in vortex breakdown, abrupt lift fluctuations and differences in aerodynamic stability when subjected to dynamic conditions. It is therefore essential

to comprehend the aerodynamic behaviors in order to enhance the design and control of contemporary high-performance aircraft.

Under the rolling motion, the unsteady effects can cause vortex asymmetry between advancing and retreating wing sides, leading to differences in the vortex core strength and also the breakdown onset. Roll rate and amplitude directly influence the breakdown location, with high roll rates producing earlier breakdown on the retreating side. Studies such as those by Lowson and Riley [4], and Gursul and Ho [5] have indicated several factors that could affect the variation of vortex breakdown position over the delta wing, including the wing's model geometry. Numerical simulations further revealed the coupled influence of roll oscillations and vortex stability, highlighting the complex phase-lag phenomena [6]. In the meantime, under the pitching motion, the unsteady aerodynamics are characterized by a phase lag between instantaneous angle of attack and aerodynamic response, which could shift vortex breakdown location and alter LEV coherence. Kumar et al. [7] experimentally investigated vortex topology changes during dynamic maneuvers of flying wings, revealing the significant deformation of vortex cores during pitch cycles. These findings align with some of the earlier observations on delta wings, confirming that unsteady pitching introduces dynamic effects that are absent in steady-state conditions [8].

Despite the advances, the comparative experimental datasets that capture both rolling and pitching effects on sharp-edged delta wings remain scarce. Such datasets are essential for the validation of the computational fluid dynamics (CFD) tools, particularly for maneuvering flight conditions. This present work addresses this gap through wind tunnel testing of a sharp-edged 65° delta wing model subjected to controlled rolling and pitching motions. The focus of the study is on the surface pressure distribution, vortex development and also breakdown behavior.

2. Methodology

The experimental investigation was conducted using a sharp-edged delta wing model with a chord length of 0.814 m and a sweep angle of 65°. The wing model was fabricated from lightweight aluminum to ensure rigidity during testing. Furthermore, a customized test rig was designed to mount the wing model inside the subsonic open-circuit wind tunnel. The rig allowed for precise adjustments of angle of attack, α and rolling motion, Φ, enabling a wide range of aerodynamic configurations to be tested. The wind tunnel has a test section with dimension of 1.2 m × 1.2 m and can be operated at a maximum velocity of 50 m/s. Figure 1 depicts the delta wing model used in this study while the test rig designed for the wind tunnel testing in this study is shown in Figure 2.

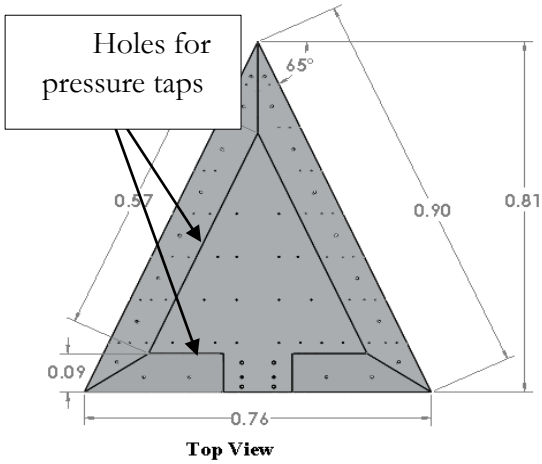

Figure 1: Dimensions of the VFE-2 delta wing model used in this study

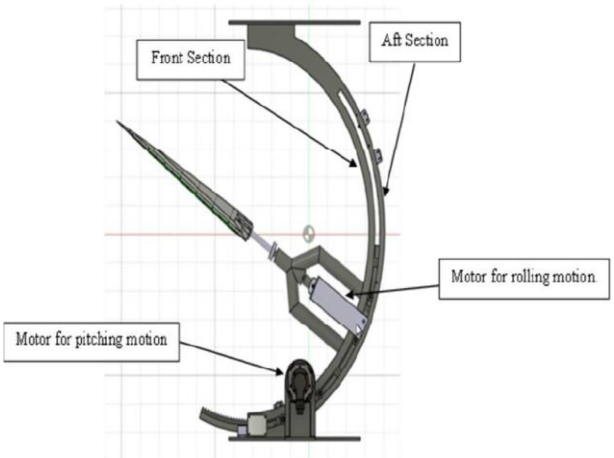

Figure 2: Wind tunnel test rig assembly for this study

The surface pressure measurements were obtained using 106 pressure taps, which were distributed across the delta wing surface to capture the detailed pressure distribution as shown in previous Figure 1. Each pressure tap was connected through flexible tubing to a 128-channel pressure scanner (accuracy of ±0.05% full-scale), interfaced with LABVIEW for real-time data acquisition as depicted in Figure 3. Moreover, the tunnel free-stream velocity was measured using a Pitot-static tube that was connected to a digital manometer. The operating temperature and static pressure were also recorded to calculate air density and viscosity. The Reynolds number for the wind tunnel tests was set at 1.288×10^6, which was corresponding to a free-stream velocity of 25 m/s at 27 °C and 1 atm.

Figure 3: LABVIEW interface for real-time data acquisition process

The experiments were carried out at angles of attack ranging from 0° to 20°, with roll angles varied systematically to study the unsteady aerodynamic behavior. Each test condition was repeated three times to ensure consistency and reproducibility. Pressure data were recorded through LABVIEW and stored in Excel for further processing. The Reynolds number, Re was computed using the relation in Equation 1, where ϱ is air density, V is free-stream velocity, L is chord length and μ is dynamic viscosity. Both air density and viscosity were determined through the data interpolation from standard air property tables at temperature, T equals 27 °C. Furthermore, the surface pressure data were then processed to compute the pressure coefficient, C_p that is defined by Equation 2, where P_s is surface static pressure, P_∞ is free-stream static pressure, ϱ_∞ is air density and V_∞ is the free-stream velocity.

$$R_e = \frac{\rho V L}{\mu} \tag{1}$$

$$C_p = \frac{P_s - P_\infty}{0.5\rho_\infty V_\infty^2} \tag{2}$$

The averaged C_p values were later sorted in an Excel spreadsheet for clarity. Subsequently, Kriging interpolation was applied using the Surfer software to estimate the C_p distributions across the delta wing surface. It should be noted that the Kriging method accounts for spatial correlations between pressure tap locations, producing smooth contour maps of the pressure distribution. In order to refine the results of the wind tunnel testing, correction methods can be applied. The tunnel blockage effects have been considered as the influence of the solid walls surrounding the finite tunnel flow on the flow field at the model [9]. For this study, the Maskell's correction [10] for tunnel blockage effects was applied.

Uncertainty analysis was also performed to quantify the reliability of the experimental results. The pressure scanner provided a measurement accuracy of ± 0.05% full scale whereas the Pitot-static tube velocity measurements had an uncertainty of ± 0.2 m/s. On the other hand, the angular positioning system allowed adjustment of angle of attack and roll with a tolerance of ± 0.1°. Repeatability checks were conducted by repeating each test condition three times and the standard deviation of C_p values was calculated to estimate the experimental scatter. Overall, the propagation of uncertainty through the C_p equation indicated a combined error of less than ± 2%. This level of accuracy was deemed sufficient for capturing aerodynamic trends of the delta wing under dynamic motions.

All in all, Figure 4 outlines the overall methodological framework for this study.

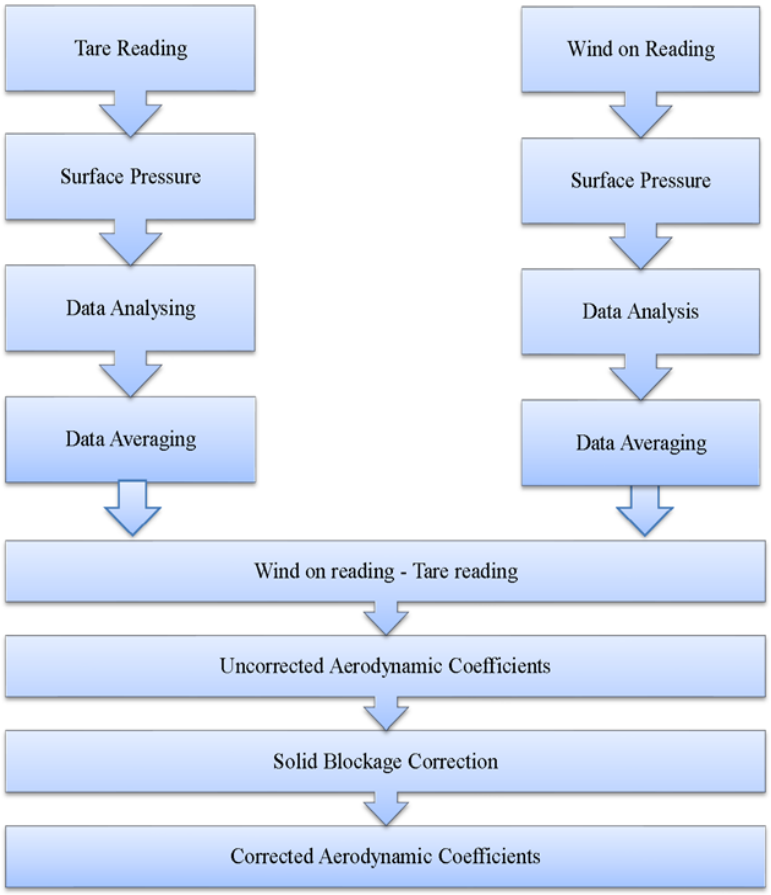

Figure 4: Overall flowchart of data collection and analysis process in this study

3. Results and Discussion

The pressure distribution in a pitching motion on the VFE-2 delta wing was investigated at angles of attack, AOA ranging from 0° to 20°. At 0°, the C_p distribution appears to remain relatively uniform, indicating the absence of any significant vortex activity. However, as AOA increased to 10°, the pressure distribution revealed the onset of the leading-edge vortex formation, which was characterized by lower pressure regions near the leading edges. This situation can be observed in Figure 5.

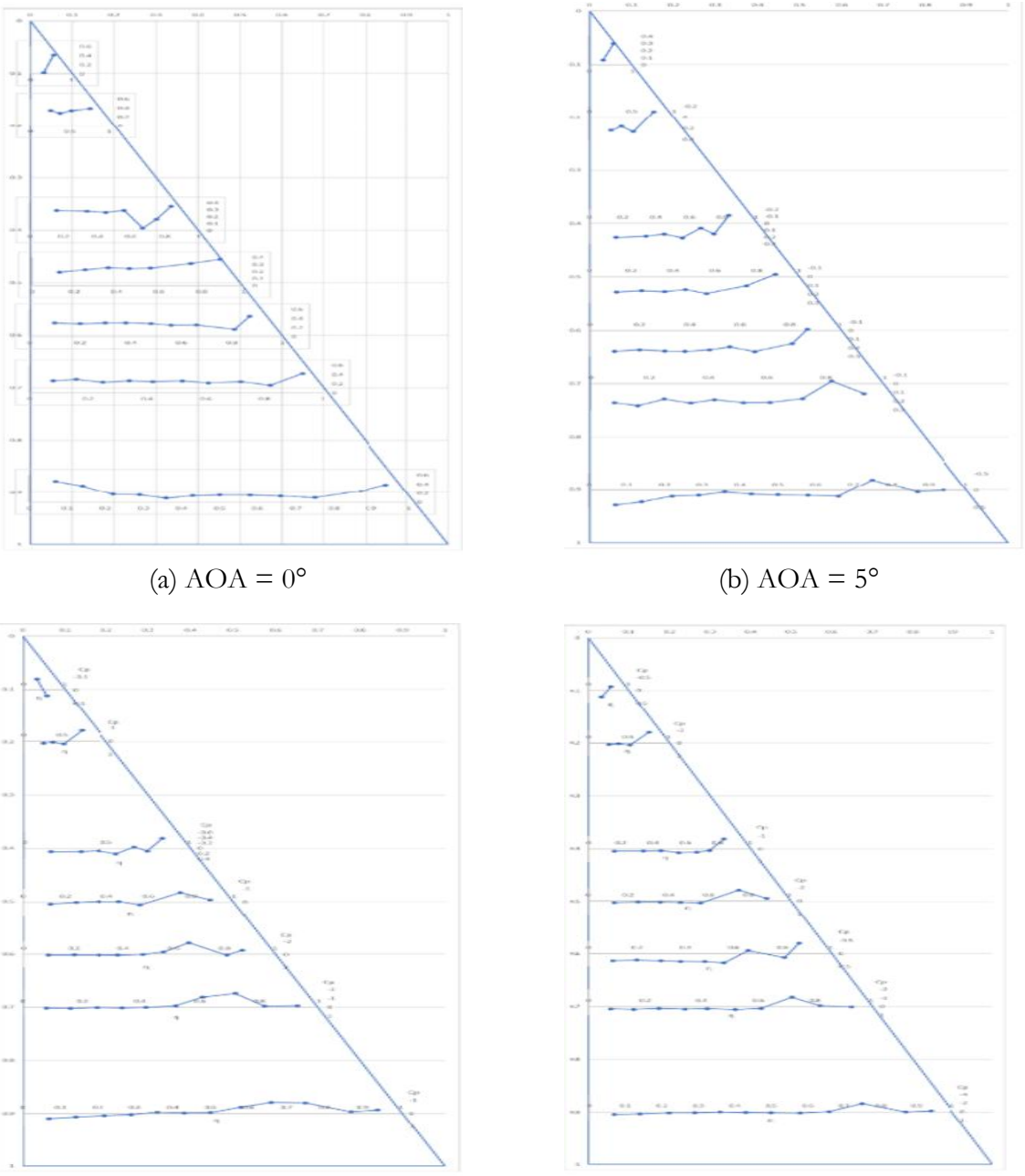

(a) AOA = 0° (b) AOA = 5°

(c) AOA = 8° (d) AOA = 10°

Figure 5: Effect of vortex formation at AOA between 0° to 10°

Furthermore, Figure 6 depicts the effects of vortex formation for the delta wing between angles of attack of 13° to 20°. At 15°, stronger suction peaks were observed along the leading edges, suggesting well-developed primary vortices. When the AOA reached 20°, the suction peaks had further intensified and extended upstream, highlighting the growth of the primary vortex system and the early emergence of the secondary vortices. These results demonstrate the progressive development of vortex-dominated flow as AOA increased. On the whole, at low AOA (i.e. between 0° to 5°), the flow remained attached with negligible vortex activity. By 10°, coherent leading-edge vortices were established, resulting in the distinct low-pressure regions. At 15°, the vortices strengthened significantly, accompanied by the wider suction footprint across the wing surface. Eventually, at 20°, the flow exhibited more complex patterns, including the development of secondary vortices closer to the wing root.

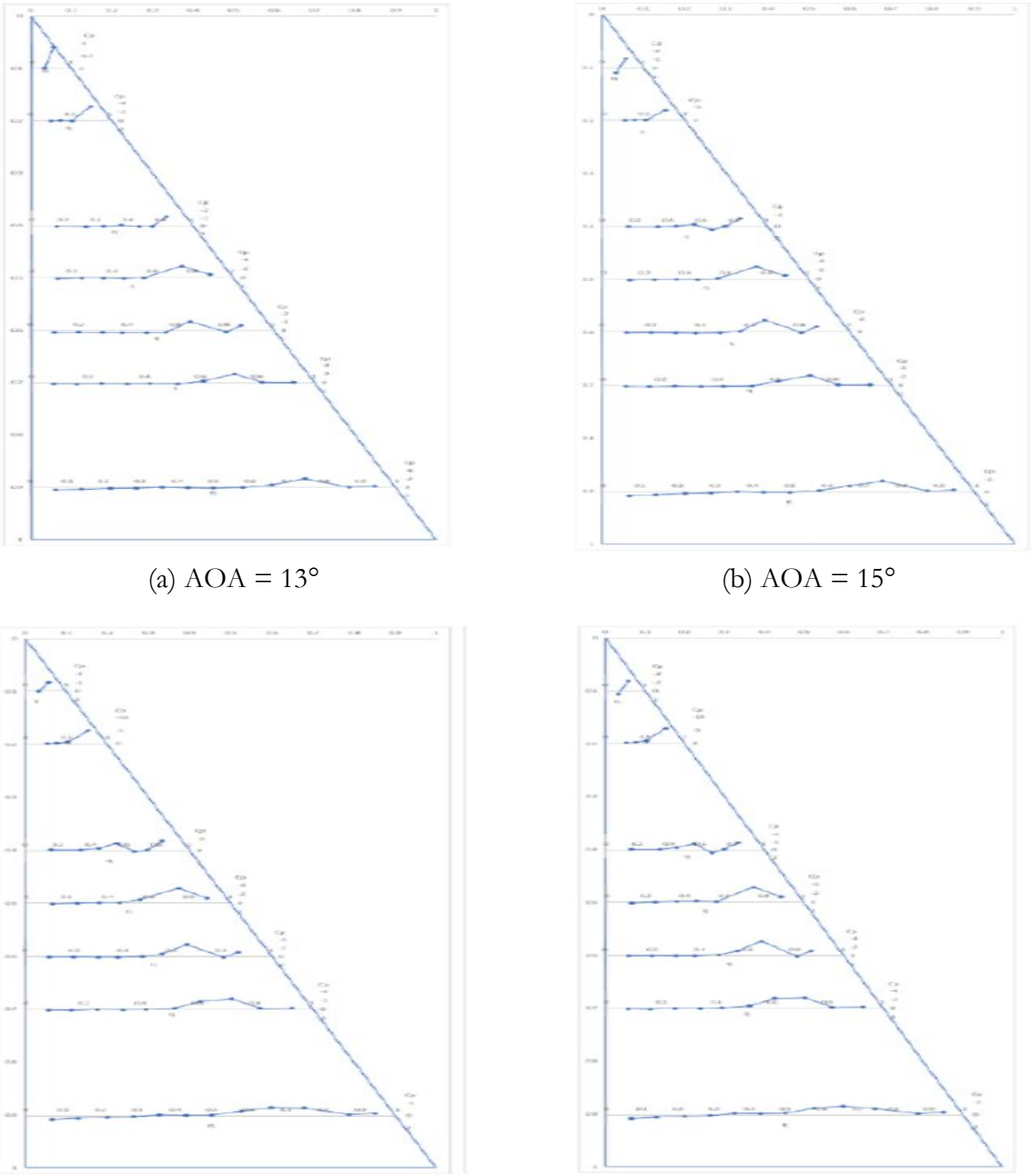

(a) AOA = 13° (b) AOA = 15°

(c) AOA = 18° (d) AOA = 20°

Figure 6: Effect of vortex formation at AOA between 13° to 20°

The obtained results confirm that both the vortex's strength and position are strongly dependent on the AOA. As the AOA increased, the primary vortex moved upstream and closer to the wing surface. In addition, the secondary vortex structures emerged, consistent with the aerodynamic behavior of the delta wing as reported in the previous studies. The flow topology was further examined using pressure contours interpolated with the Kriging method. This approach allowed detailed visualization of pressure distributions across the wing surface beyond the limits of the discrete pressure tap measurements. The contour plots, as shown in Figure 7, demonstrated that at higher AOAs, the suction region expanded toward the root and shifted upstream. At 20°, the contours indicated a progressive upstream migration of both primary and secondary vortex cores. The use of the Kriging interpolation provided continuous representations of the pressure field, thereby enhancing the interpretation of the vortex interaction and breakdown phenomena.

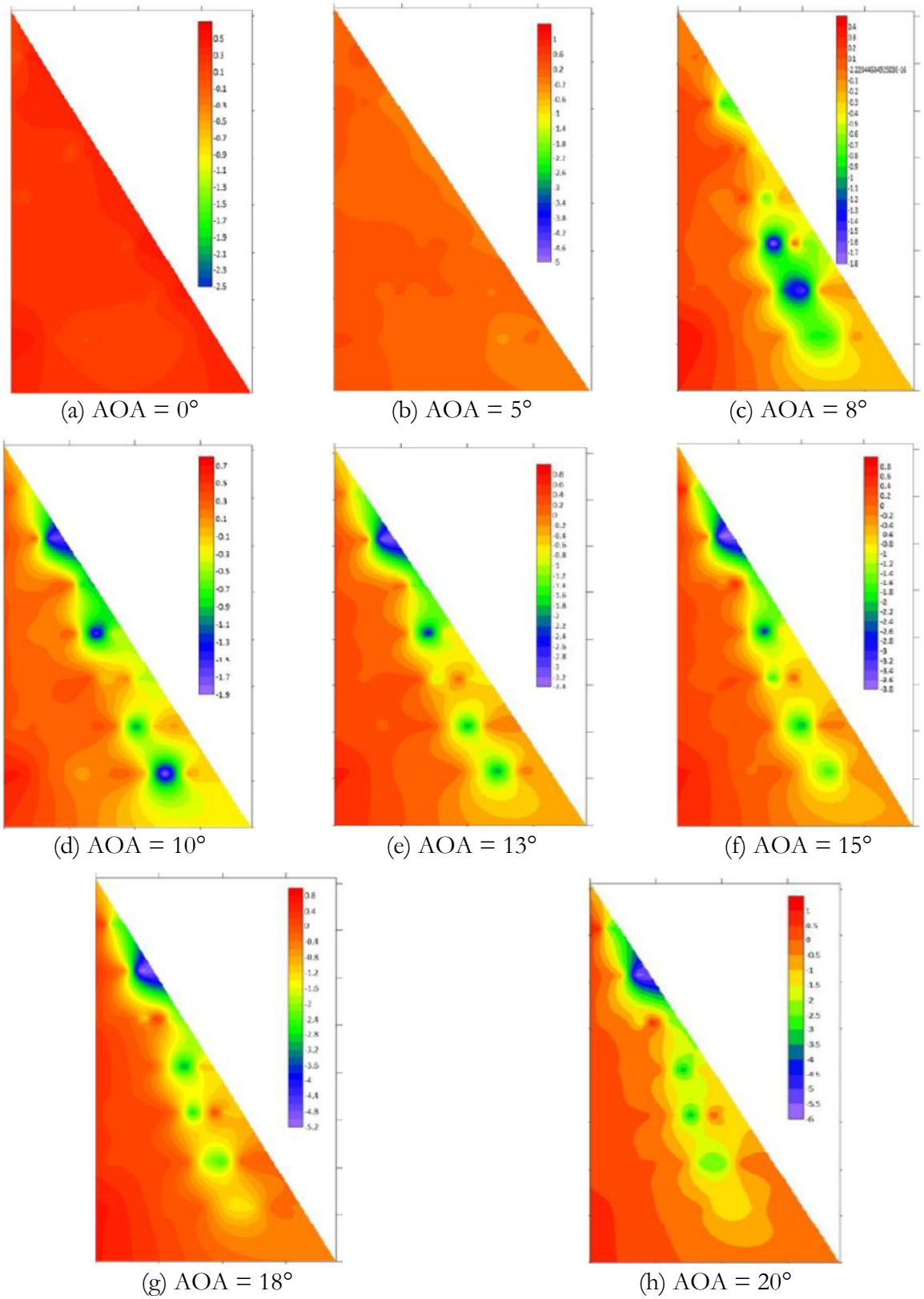

(a) AOA = 0° (b) AOA = 5° (c) AOA = 8°

(d) AOA = 10° (e) AOA = 13° (f) AOA = 15°

(g) AOA = 18° (h) AOA = 20°

Figure 7: Flow topology at AOA ranging between 0° to 20°

All in all, the experimental findings highlighted several key aerodynamic characteristics of the VFE-2 delta wing as listed as follow:

- **Primary vortex development:** Initiated at moderate AOA (≈10°), intensifying with the increasing angle.
- **Upstream shift:** At higher AOAs, the primary vortex migrated upstream and moved closer to the wing surface.
- **Secondary vortex formation:** The secondary vortices emerged at 20°, contributing to the increased flow complexity.
- **Vortex breakdown tendency:** The upstream shift and intensification of vortices at 20° suggest the onset of vortex breakdown, consistent with delta wing flow theory.

Overall, the results align with previous aerodynamic studies, confirming that the sharp-edged delta wing maintains strong vortex lift at high AOAs but also prone to the flow instability and breakdown at extreme conditions.

In the meantime, for rolling motions, Figure 8 shows the experimental results for the sharp-edged delta wing subjected to a constant roll angle, Φ of 10° and AOA ranging from 0° to 20°. Freestream pressure was used as the reference condition across all experiments, serving as the tare values for data normalization. The results are discussed in terms of C_p distributions and contour plots to highlight the influence of angle of attack and rolling motion on the flow behavior. In Figure 8, at AOA of 0°, the C_p distribution across the span appears to be nearly symmetric. A slight increase in pressure occurred near the nose whereas the gradual decrement towards the tips resulted in small negative C_p values. With the application of roll, the outer wing showed marginally lower pressure while the inner wing experienced a higher pressure. The resulting asymmetry was weak but established the basis of roll-induced pressure differentials. When AOA was 5°, suction increased near the leading edge and the outer wingtip showed stronger negative C_p while the inner wing retained higher pressure. At AOA of 8°, the low-pressure region expanded, appearing earlier along the chord ($x/c \approx 0.2$). Moreover, at AOA of 10°, the pressure asymmetry further intensified, with the outer wingtip experiencing the maximum suction and the inner wing showing elevated positive pressure. These indicated the strengthening of the leading-edge vortices with increasing incidence, amplified by the roll-induced inclination. Furthermore, at AOA of 13°, the pressure distributions revealed sharp reductions near the leading edge ($x/c = 0.2$ to 0.4). This behavior was in correspondent to the development of the coherent leading-edge vortices, which sustained lift by generating strong suction above the wing. A slight pressure recovery is observed near the trailing edge, linked to wake formation. The contours confirmed an enhanced vortex activity, with strong asymmetry between the outer and inner wing. Moving to when AOA was 15°, strong suction at the nose ($x/c \approx 0.1$) signified a vortex-dominated flow. This condition coincided with the onset of vortex breakdown reported for sharp-edged delta wings at high Reynolds numbers. The contours revealed enlarged low-pressure regions, particularly on the outer wing due to the rolling motion. At AOA of 18°, the negative pressure peak reduced slightly despite the higher incidence, suggesting the destabilization of the leading-edge vortices. Rolling further sheared the vortex structures, producing broader but less coherent low-pressure regions. Finally, at the maximum tested incidence where AOA was 20°, the pressure coefficient reached its lowest values across the wing. Extensive low-pressure regions in the contour plots marked the vortex breakdown and collapse. This stage was associated with the significant lift loss and increased drag, representing severe aerodynamic instability. Across the tested range, three different regimes can be identified as listed below:

- **Low incidence (i.e. AOA < 5°)** – nearly symmetric distributions, weak roll effect.
- **Moderate incidence (i.e. AOA between 5° and 10°)** – strong suction, coherent vortices, roll-induced asymmetry.
- **High incidence (i.e. AOA ≥ 13°)** – vortex-dominated flow transitioning into breakdown; rolling accelerates asymmetry and destabilization.

Overall, the rolling motion at Φ = 10° can be seen to consistently enhance the pressure asymmetry across the wingspan. While this contributes to the roll control effectiveness at moderate AOA, it also accelerates vortex breakdown at higher incidence, degrading aerodynamic stability.

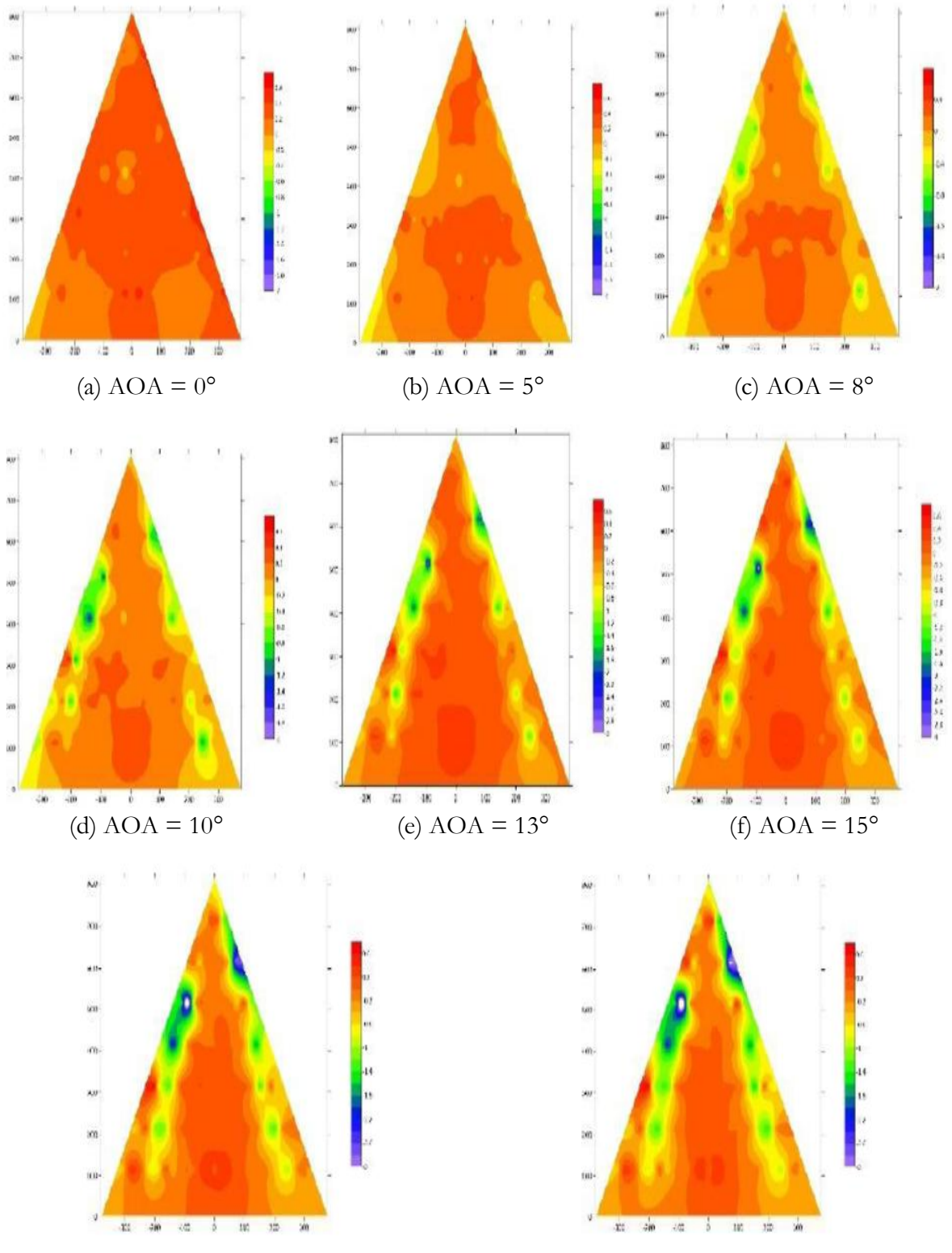

(a) AOA = 0° (b) AOA = 5° (c) AOA = 8°

(d) AOA = 10° (e) AOA = 13° (f) AOA = 15°

(g) AOA = 18° (h) AOA = 20°

Figure 8: Pressure coefficient characteristics at different AOA for Φ = 10°

4. Conclusion

This study experimentally investigated the aerodynamic behavior of the sharp-edged VFE-2 delta wing under both pitching and rolling motions. The results have provided important insights into the effects of AOA and dynamic motion on the vortex flow topology, pressure distribution and the overall aerodynamic performance. For the pitching motion experiments, the findings have demonstrated that AOA has dominant influence on the vortex development. At lower AOAs (i.e. AOA $\leq 5°$), the flow remained attached with minimal vortex activity. With increasing AOA, flow separation initiated at the leading edge, forming the primary vortices whose position and strength evolved along the chord. The primary vortex strengthened and moved upstream with higher AOA while vortex breakdown occurred at the trailing edge for high AOAs (i.e. AOA $\geq 18°$). Weak secondary vortices were observed in some cases, particularly at AOA of 8°, 18° and 20°. The conducted pressure contour analyses confirmed that vortex strength and breakdown location are closely linked to AOA, with the breakdown characterized by the disappearance of suction peaks and loss of coherent vortex structure. Meanwhile, for the rolling motion case at Φ of 10°, the pressure coefficient was observed to decrease as AOA increased due to the destabilization and breakdown of the leading-edge vortices. Rolling motion amplified asymmetries in the vortex system, making breakdown more likely even at moderate AOA. The reduction in lift and increase in drag were attributed to vortex disruption and wake formation. Differences in the pressure coefficient were more pronounced at higher AOA, indicating that the rolling motion strongly influences vortex stability. On the whole, from a design perspective, these results suggest that sharp-edged delta wings exhibit stable vortex behavior at the lower AOA under both pitching and rolling motions. Stable operation has been observed up to approximately AOA of 8° at 25 m/s of free-stream velocity. Beyond this range, vortex breakdown dominates the flow, leading to aerodynamic performance penalties. These findings provide valuable guidance for the aerodynamic design and control of delta-wing configurations operating in dynamic flight conditions.

Acknowledgement

The authors would like to thank the Aeronautics Laboratory, Universiti Teknologi Malaysia (UTM) for their support in this research activity.

References

[1] I. Gursul, 'Review of Unsteady Vortex Flows Over Delta Wings', Presented at AIAA Applied Aerodynamics Conference, Orlando, USA, 2003.

[2] I. Gursul, R. Gordnier and M. Visbal, 'Unsteady Aerodynamics of Nonslender Delta Wings', Progress in Aerospace Sciences, vol. 41, no. 7, pp. 515-557, 2005.

[3] M. F. A. Zamzuddin, M. Said, N. A. Musa, K. A. Kasim and S. Mat, 'Analysis of Vortex on Sharp-edged Delta Wing with Blowing Effect', Journal of Transport System Engineering, vol. 10, no. 1, pp. 14-23, 2023.

[4] M. V. Lowson and A. J. Riley, 'Vortex Breakdown Control by Delta Wing Geometry', Journal of Aircraft, vol. 32, no. 4, pp. 832-838, 1995.

[5] I. Gursul and C. M. Ho, 'Vortex Breakdown Over Delta Wings in Unsteady Freestream', AIAA Journal, vol. 32, no. 2, pp. 433-436, 1994.

[6] M. Sereez, M. Goman, N. Abramov and C. Lambert, 'Numerical Simulation of Self-Sustained Roll Oscillations of an 80-Degree Delta Wing Caused by Leading-Edge Vortices', Aerospace, vol. 12, no. 3, 197, 2025.

[7] V. Kumar, A. C. Mandal and K. Poddar, 'An Experimental Investigation on the Aerodynamic Characteristics and Vortex Dynamics of a Flying Wing', The Aeronautical Journal, vol. 128, no. 1326, pp. 1681-1705, 2024.

[8] I. Gursul, R. Gordnier and M. Visbal, 'Unsteady Aerodynamics of Nonslender Delta Wings', Progress in Aerospace Sciences, vol. 41, no. 7, pp. 515-557, 2005.

[9] S. Wiriadidjaja, A. S. Mohd Rafie, F. I. Romli and O. K. Ariff, 'Aerodynamic Interference Correction Methods Case: Subsonic Closed Wind Tunnels', Applied Mechanics and Materials, vol. 225, pp. 60-66, 2012.

[10] J. E. Hackett and K. R. Cooper, 'Extensions to Maskell's Theory for Blockage Effects on Bluff Bodies in a Closed Wind Tunnel', The Aeronautical Journal, vol. 105, no. 1050, pp. 409-418, 2001.